



<http://www.diva-portal.org>

## Postprint

This is the accepted version of a paper presented at *2025 International Electric Machines and Drives Conference-IEMDC-Annual, MAY 18-21, 2025, Houston, TX.*

Citation for the original published paper:

Böcker, L., Ayaz, E., Peretti, L. (2025)

Minimizing Losses in Electric Drivetrains: A Comparative Analysis of Inverter Topologies, Switching Frequencies, and Modulation Techniques

In: *2025 IEEE International Electric Machines & Drives Conference (IEMDC)* (pp. 853-858). Institute of Electrical and Electronics Engineers (IEEE)

IEEE International Conference on Electric Machines and Drives

<https://doi.org/10.1109/IEMDC60492.2025.11061021>

N.B. When citing this work, cite the original published paper.

© 2025 IEEE. Personal use of this material is permitted. Permission from IEEE must be obtained for all other uses, in any current or future media, including reprinting/republishing this material for advertising or promotional purposes, creating new collective works, for resale or redistribution to servers or lists, or reuse of any copyrighted component of this work in other works.

Permanent link to this version:

<http://urn.kb.se/resolve?urn=urn:nbn:se:kth:diva-374650>

# Minimizing Losses in Electric Drivetrains: A Comparative Analysis of Inverter Topologies, Switching Frequencies, and Modulation Techniques.

Lukas Böcker

*KTH Royal Institute of Technology*  
Stockholm, Sweden  
lbocker@kth.se

Enes Ayaz

*KTH Royal Institute of Technology*  
Stockholm, Sweden  
enesa@kth.se

Luca Peretti

*KTH Royal Institute of Technology*  
Stockholm, Sweden  
lucap@kth.se

**Abstract**—This paper investigates the impact of switching frequency and modulation technique on the efficiency of electric drivetrains utilizing inverter-driven Permanent Magnet Synchronous Machines, focusing on heavy-vehicle applications. Accounting for inverter conduction and switching losses, along with machine copper, iron, and magnet losses, a comparison between two- and three-level inverters is performed at key operating points relevant to long-haul truck applications. This study employs current-based finite element analysis for machine loss estimation and a virtual prototyping method for inverter loss estimation to analyze drivetrain efficiency. The findings indicate that there is an optimal switching frequency evidently improving overall efficiency. Moreover, the system using the three-level inverter demonstrates notably lower system losses.

**Index Terms**—Electric Drivetrains, Permanent Magnet Synchronous Machines, Pulse Width Modulation, Multilevel Inverters, Switching Frequency, Modulation Techniques, Energy Efficiency

## I. INTRODUCTION

Permanent Magnet Synchronous Machines (PMSMs) gained increasing popularity for the use in electric drivetrains, especially for heavy vehicle applications, thanks to their ability to meet high torque density and efficiency requirements. Driving PMSMs by Pulse Width Modulation (PWM) inverters, allows for precise speed and torque control. When evaluating the overall combined drivetrain energy efficiency, it is important to consider losses in both the electric machine and the inverter. Both have been widely studied, with numerous models and calculation methods developed to evaluate them accurately [1]–[6]. Furthermore, it has been shown that additional harmonic losses induced in PMSMs when driven by a PWM source can significantly impact the overall efficiency and, therefore, cannot be neglected [7]–[10].

The loss estimation inside PMSMs caused by PWM operation has been addressed using analytical as well as simulation-based methods [7]–[10]. In [11], work has been carried out on choosing the optimal inverter topology to minimize the additional iron losses. The impact of different modulation techniques and varying switching frequencies on iron and magnet losses respectively has been investigated in [12], [13].

While above mentioned methods aim to minimize losses in inverters and PMSMs individually, a holistic approach, taking

into consideration both loss contributing components, is essential to ultimately improve overall drivetrain energy efficiency. This is especially important, as the relationship between the harmonic components in PMSMs and inverter switching frequency poses a trade-off [14]. While higher switching frequencies lead to an increase in inverter switching losses, the PMSM's inductance more effectively filters out current ripples at those higher switching frequencies, thereby reducing PWM-related losses in the PMSM [15]. In [16] an optimization study investigates the effect of a variable switching frequency and different modulation methods on drivetrain losses using a two-level inverter topology. The results confirm that the choice of switching frequencies impacts energy efficiency across the operational range of the drivetrain system, thereby highlighting that aforementioned trade-off should be taken into account during inverter design. However, the loss estimation in [16] is performed analytically to allow for rapid evaluation, which consequently results in a reduction of accuracy.

This study investigates the influence of different switching frequencies and modulation methods on the overall drivetrain efficiency. It presents an analysis of a system using a two-level inverter topology and extends this analysis to include a three-level inverter topology, thus allowing for a direct comparison between the two. The diverse range of operating points during vehicle operation presents challenges for optimization. Given the primary focus on long-haul truck applications, the scope is narrowed to a comparison of six operating points that account for the majority of energy consumption within a typical driving cycle. This, in contrast to [16], allows for a more precise estimation of PMSM losses through current-based finite element analysis (FEA) simulations, similar to the approach taken in [9]. Inverter losses are estimated using a virtual prototyping method which incorporates figure-of-merit parameters [17], enabling accurate system-level modeling without specifying a particular semiconductor device.

The remaining part of the paper is structured as follows: Section II lays out the system specifications, followed by a detailed description of the modeling approach in Section III. Finally, Section IV presents the results.

## II. SYSTEM SPECIFICATIONS

This study compares the losses of a PMSM drive fed by either a 2-level voltage source inverter (VSI) or a 3-level neutral point clamped VSI, which are both illustrated in Fig. 1.

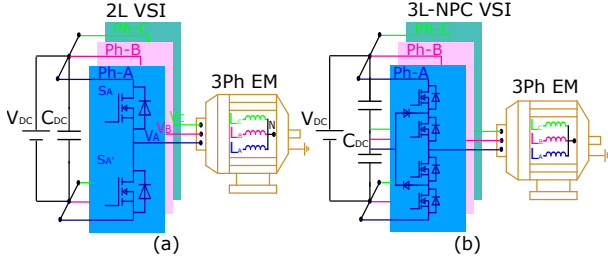


Fig. 1. The evaluated inverter topologies. (a) 2-level VSI. (b) 3-level neutral point clamped VSI.

The power rating of the machine is 350 kW and the DC-link voltage of the system is 625 V. Fig. 2 displays the torque-speed operating map of the PMSM. Given the long-haul truck application of the drive, most of the energy during a representative driving cycle is consumed around a few distinct operating points, allowing the scope of this work to be narrowed down to the analysis of six key operating points, as shown in Fig. 2. Torque and speed values for each operating point are provided in Table I.

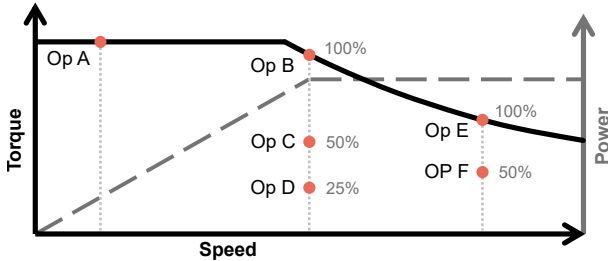


Fig. 2. Torque over speed map including the investigated operating points.

TABLE I

TORQUE, SPEED AND CURRENTS FOR THE SELECTED OPERATING POINTS.

OP:	A	B	C	D	E	F
Speed [rpm]	200	3 000	3 000	3 000	5 000	5 000
Torque [Nm]	1 250	1 240	620	310	740	370
$i_d$ [A]	-565	-689	-254	-92	-774	-469
$i_q$ [A]	571	458	319	193	200	119

## III. MODELING APPROACH

The modeling approach utilizes a co-simulation setup to estimate the overall system losses. Fig. 3 illustrates the structure of the deployed simulation process. The entire system including the inverter, machine, and a closed-loop control is modeled in a *Simulink* environment to extract the phase current waveforms in the machine based on operating point and PWM

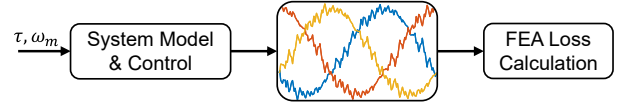


Fig. 3. Simulation flowchart.

switching frequency. Once the system reaches steady state for a specific operating point, the current waveforms for one electrical period are extracted. Note that at this stage, these currents contain harmonics, which will induce higher losses in the FEA analysis compared to pure sinusoidal inputs. They are then used as an input for transient current source FEA simulations to compute the losses in the PMSM.

### A. Machine Model

To achieve a high level of detail, the PMSM is modeled with flux linkage maps in the dq reference frame. These maps are obtained prior from FEA simulations and account for magnetic saturation as well as cross-saturation. The flux linkage maps are obtained for varying rotor positions and then averaged (see Fig. 4). Implementing the flux linkage maps as lookup tables, the flux linkage  $\psi$  can be calculated as a function of the dq currents,  $\psi_d(i_d, i_q)$  and  $\psi_q(i_d, i_q)$ . The dq voltage equations of the PMSM using flux linkages are expressed as:

$$\begin{cases} v_d = R_s i_d + \frac{d\psi_d}{dt} - \omega_e \psi_q \\ v_q = R_s i_q + \frac{d\psi_q}{dt} + \omega_e \psi_d \end{cases} \quad (1)$$

As the flux linkages become the state variables for the implemented machine model, it is necessary to express the dq-axis currents as functions of the flux linkages,  $i_d(\psi_d, \psi_q)$  and  $i_q(\psi_d, \psi_q)$ . This is achieved by computing the inverse of the flux linkage maps using a method similar to that outlined in [18] and shown in Fig. 5.

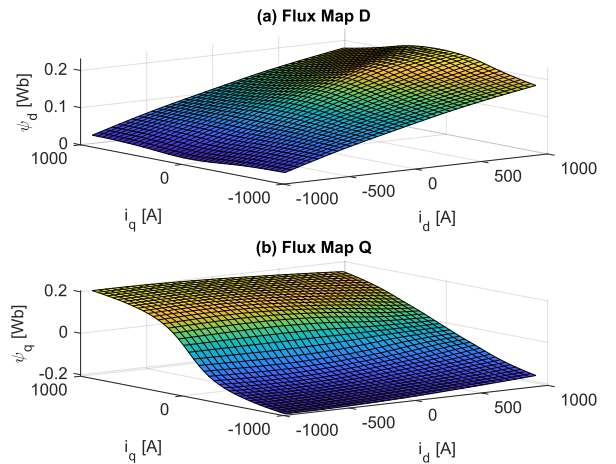


Fig. 4. Flux Linkage maps for d- and q-axis direction.

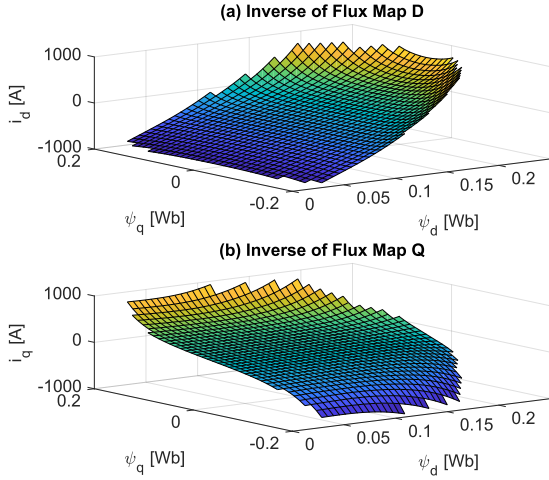


Fig. 5. Inverse of the Flux Linkage maps for d- and q-axis direction.

### B. Control

To obtain the required current waveforms for the FEA-based loss calculation corresponding to the targeted speed and torque values of each operating point, the dq axis current reference values are determined using an offline calculation-based field weakening control method as described in [19]. The values of the reference currents are stored in torque-speed lookup tables as depicted in Fig. 6.

A closed-loop field oriented control scheme is implemented to control the currents. The reference currents for the specified operating points are given in Table I. A simplified version of the implemented model and control setup is shown in Fig 7.

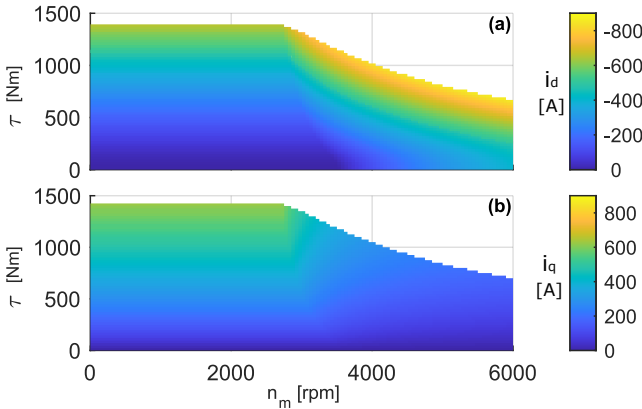


Fig. 6. Currents depending on operating point. (a)  $i_d$ . (b)  $i_q$ .

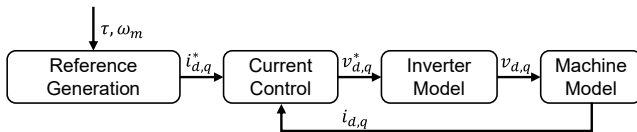


Fig. 7. Simplified model and control structure.

### C. Inverter Model

The inverter is modeled by implementing the carrier-based PWM principles described in [20] for sinusoidal (SPWM) and third harmonic injection PWM (THPWM). While a single triangular carrier is used for the two-level VSI, level-shifted dual carrier signals are implemented to achieve three-level inverter modulation. The switching frequency is varied from 5 kHz to 30 kHz.

### D. FEA Simulation Setup

Transient current-source FEA simulations compute the PMSM losses by applying the phase current waveforms derived from *Simulink*. The simulations are conducted using *COMSOL Multiphysics*. To analyze the high frequency contents resulting from the PWM switching, the simulation has to be set up accordingly. Looking at the FFT analysis of the currents (see Fig. 8), it becomes obvious that the main harmonic components are to be expected around the integer multiples of the switching frequency with side bands located around these frequencies. Beyond 150 kHz the harmonic contribution becomes negligibly small. Therefore, the analysis is limited to a frequency of 150 kHz. To include and resolve this frequency, the time step size for solving the simulation has to be set sufficiently small. According to the Nyquist criterion, the simulation time step must be small enough that its corresponding sampling frequency is at least twice the maximum frequency of interest. Based on this requirement, the maximum time step for the simulation is set to 1e-6 s, resulting in a Nyquist frequency of 500 kHz.

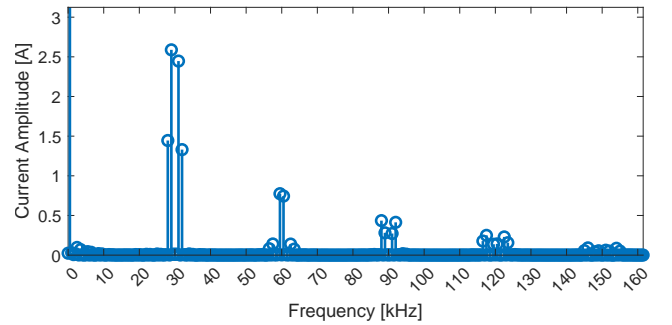


Fig. 8. FFT of phase current at OP F and switching frequency of 30 kHz.

### E. Loss Modeling

PMSM losses are categorized into copper, magnet, and iron losses. The copper losses consist of a resistive DC component, and an AC component caused by the skin effect. The magnet losses primarily result from eddy currents induced by the time-varying magnetic field. Both loss types are computed in *COMSOL*, which calculates the cycle-averaged loss density  $Q$  as:

$$Q_{copper/magnet} = \frac{1}{T} \int_{T_{end}-T}^{T_{end}} \mathbf{J} \cdot \mathbf{E} dt \quad (2)$$

where  $T$  is the electrical period,  $J$  the current density and  $E$  the electrical field. The iron losses require post-processing, and they are calculated applying the Bertotti model as:

$$P_{iron} = k_h B^{\alpha_h} f + k_e B^{\alpha_e} f^2 + k_x B^{\alpha_x} f^{1.5} \quad (3)$$

where  $f$  is the frequency and  $B$  is the magnetic flux density respectively. The parameters used in (3) are specified in Table II.

TABLE II  
IRON LOSS PARAMETERS

Loss Type	Loss Constant [ $W/m^3$ ]	Exponent [-]
Hysteresis	$k_h = 279$	$\alpha_h = 2$
Eddy Currents	$k_e = 0.606$	$\alpha_e = 2$
Excess	$k_x = 2.37$	$\alpha_x = 1.5$

The inverter losses in 2-level 3-phase (2L-3Ph) and 3-level neutral point clamped (3L-NPC) inverters are estimated using a virtual prototyping method that utilizes figure-of-merit (FOM) parameters to evaluate semiconductor losses. This method enables a thorough system-level analysis without relying on specific semiconductor device data. A detailed description can be found in [21].

Semiconductor losses in inverters are mainly divided into two types: conduction losses and switching losses. These losses are influenced by factors such as the inverter topology, switching frequency, and the specific characteristics of the semiconductor devices used.

Firstly, conduction losses occur when the semiconductor devices are in the on-state, allowing current to flow through them. The conduction loss for a single switch is calculated using the following equation:

$$P_c = \frac{1}{2\pi} \int_{\theta_{C1}}^{\theta_{C2}} r_{ds} \cdot i_{ds}(\theta)^2 \cdot D(\theta) d\theta \quad (4)$$

where  $r_{ds}$  is on-state resistance of the switch,  $i_{ds}(\theta)$  is the current through the switch as a function of the phase angle,  $D(\theta)$  the duty cycle of the switch,  $\theta_{C1}$  and  $\theta_{C2}$  are the conduction angles. The on-state resistance  $r_{ds}$  is affected by the voltage rating  $V_B$  and the die area of the semiconductor device  $A_{die} = 500 \text{ mm}^2$ . It can be approximated as:

$$r_{ds} = \frac{k_R \cdot V_B^{\alpha_r}}{A_{die}} \quad (5)$$

where  $k_r = 7.2e^{-3} \frac{m\Omega \cdot mm^2}{V^{1.6}}$  and  $\alpha_r = 1.6$  are technology-dependent coefficients. When calculating conduction losses, the impact of the body diode might be disregarded during the reverse conduction of MOSFETs and dead times. However, neglecting the body diode results in an overestimation of losses during reverse conduction and an underestimation of losses during dead times, as noted in [22]. These opposing effects tend to partially offset each other.

Secondly, switching losses occur during the transition between the on and off states of the semiconductor devices. These losses originate from two primary components: zero

current switching (ZCS) energies and overlapping energies. The zero current switching energy  $E_{sw-ZCS}$  is estimated as:

$$E_{sw-ZCS} = C_{oss,Q}(V_{sw})V_{sw}^{\alpha_c} = k_c U_b^{\alpha_c} A_{die} V_{sw}^2 \quad (6)$$

where  $C_{oss,Q}$  is the output capacitance of the switch,  $V_{sw}$  is the switching voltage,  $k_c = 1.6e^4 \frac{pF \cdot V}{mm^2}$  and  $\alpha_c = -1$  are technology-dependent coefficients. The overlapping switching energy  $E_{sw-OL}$  is calculated as:

$$E_{sw-OL} = \left( \frac{V_{sw} I_{sw}^2}{2 \frac{di}{dt_{on}}} + \frac{V_{sw}^2 I_{sw}}{2 \frac{dv}{dt_{on}}} \right) + \left( \frac{V_{sw} I_{sw}^2}{2 \frac{di}{dt_{off}}} + \frac{V_{sw}^2 I_{sw}}{2 \frac{dv}{dt_{off}}} \right) \quad (7)$$

where  $dv/dt = 20 \frac{kV}{\mu s}$  is the voltage change rate and  $di/dt$  is the current change rate during switching. These rates are significantly higher for SiC devices, enabling faster switching and reduced energy loss.

The total switching losses  $P_{sw}$  are calculated by integrating the switching energy over the switching angles  $\theta_{sw1}$  to  $\theta_{sw2}$ :

$$P_{sw} = \frac{f_{sw}}{2\pi} \int_{\theta_{sw1}}^{\theta_{sw2}} (E_{sw-OL}(\theta) + E_{sw-ZCS}(\theta)) d\theta \quad (8)$$

Additionally, the three-level topology includes diodes connected to the midpoint of the capacitors, which also contribute to the overall losses. The switching losses of these diodes might be ignored when SiC Schottky diodes are utilized. The diode conduction losses are calculated by:

$$P_d = \frac{1}{2\pi} \int_{\theta_{D1}}^{\theta_{D2}} V_{on} \cdot i_{ds}(\theta) \cdot D(\theta) d\theta \quad (9)$$

where  $V_{on}$  is diode on-state voltage drop,  $i_{ds}$  is the current through the diode,  $\theta_{D1}$  and  $\theta_{D2}$  are diode conduction angles. Unlike MOSFETs, the diode has an additional voltage drop  $v_o$ . The on-state voltage drop  $V_{on}$  is estimated as:

$$V_{on} = r_d \cdot I_d + v_o = \frac{1}{A_{die}} (\alpha_d \cdot V_{db}^{2.5} + \beta_d) \cdot I_d + v_o \quad (10)$$

with the on-state resistance of the diode  $r_d$ , the diode blocking voltage  $V_{db}$ , the opening voltage of the diode  $v_o = 0.4 \text{ V}$ , and  $\alpha_d = 649.6e^{-6} \frac{\Omega \cdot mm^2}{V^{2.5}}$  and  $\beta_d = 202.2e^{-3} \Omega \cdot mm^2$  being technology dependent coefficients.

The conduction and switching angles for switches and diodes are needed to compute overall semiconductor losses. The angles differ depending on the specific topology, as can be found in [22]–[24].

#### IV. RESULTS

The calculated PMSM loss results for all operating points considering both the 2-level and 3-level inverters operated with SPWM and THPWM are given in Table III. The corresponding inverter losses are shown in Table IV. The inverter loss evaluation focuses on the fundamental current component, since the current ripple is negligibly small. Therefore, for a given modulation index, SPWM and THPWM give nearly identical inverter losses if the switching frequency and fundamental current remain unchanged. Using the 2-level inverter, THPWM operation gives slightly lower PMSM losses than SPWM. However, this trend reverses in the 3-level inverter scenario,

TABLE III  
SUMMED PMSM LOSSES IN [W].

2-Level	A		B		C		D		E		F	
	$f_{sw}$	SPWM	THPWM	SPWM	THPWM	SPWM	THPWM	SPWM	THPWM	SPWM	THPWM	SPWM
5 kHz	3 179	3 181	11 324	10 804	6 365	6 050	4 724	4 587	20 049	19 645	11 765	11 579
10 kHz	3 068	3 068	10 552	10 316	5 802	5 695	4 237	4 176	19 559	19 353	11 390	11 227
15 kHz	3 023	3 023	10 260	10 127	5 606	5 553	4 056	4 025	19 324	19 220	11 122	11 074
20 kHz	2 995	2 995	10 091	10 008	5 492	5 457	3 944	3 932	19 219	19 154	11 014	10 987
25 kHz	2 985	2 984	9 995	9 942	5 424	5 397	3 870	3 872	19 140	19 089	10 952	10 929
30 kHz	2 974	2 974	9 948	9 897	5 358	5 330	3 824	3 827	19 088	19 041	10 907	10 875

3-Level	A		B		C		D		E		F	
	$f_{sw}$	SPWM	THPWM	SPWM	THPWM	SPWM	THPWM	SPWM	THPWM	SPWM	THPWM	SPWM
5 kHz	3 116	3 128	9 774	10 081	5 064	5 298	3 611	3 803	18 897	19 139	10 630	10 826
10 kHz	3 042	3 047	9 573	9 740	4 925	5 083	3 494	3 623	18 764	18 898	10 540	10 697
15 kHz	3 011	3 013	9 508	9 639	4 877	5 013	3 453	3 570	18 705	18 814	10 514	10 642
20 kHz	2 991	2 993	9 467	9 583	4 845	4 968	3 425	3 537	18 671	18 771	10 489	10 610
25 kHz	2 980	2 980	9 438	9 544	4 829	4 938	3 404	3 512	18 648	18 740	10 469	10 581
30 kHz	2 970	2 971	9 426	9 516	4 805	4 905	3 387	3 487	18 632	18 712	10 451	10 550

TABLE IV  
INVERTER LOSSES IN [W] OVER SWITCHING FREQUENCY  $f_{sw}$ .

2-Level	A	B	C	D	E	F
5 kHz	1 096	1 156	362	159	1 093	474
10 kHz	1 449	1 521	527	260	1 446	675
15 kHz	1 802	1 891	698	366	1 798	870
20 kHz	2 155	2 256	863	467	2 150	1 067
25 kHz	2 508	2 620	1 028	568	2 501	1 264
30 kHz	2 861	2 991	1 199	674	2 852	1 462

3-Level	A	B	C	D	E	F
5 kHz	1 410	1 263	460	217	1 215	572
10 kHz	1 574	1 436	540	270	1 384	659
15 kHz	1 738	1 610	620	323	1 549	747
20 kHz	1 900	1 784	700	375	1 719	840
25 kHz	2 066	1 955	777	428	1 883	927
30 kHz	2 230	2 132	860	481	2 053	1 015

where the PMSM losses slightly increase for THPWM operation when compared to SPWM. Overall, the PMSM losses decrease exponentially with increasing switching frequencies due to reduced current ripples. On the contrary, the inverter losses show a linear increase with an increase in switching frequency.

In the 2-level inverter, switching losses are a dominant factor, leading to lower offsets but a steeper increase at higher switching frequencies. In contrast, the 3-level inverter experiences higher conduction losses due to series transistors, while their reduced switching voltage lowers switching losses, reducing the total losses for higher switching frequencies.

The combined evaluation of inverter and PMSM losses reveals that there is an optimal switching frequency to minimize total losses of the system. The optimal switching frequency along with the corresponding minimum combined system losses is summarized in Table V. Depending on the operating point, inverter topology, and PWM strategy the optimal switching frequency varies between 5 kHz and 19 kHz.

TABLE V  
OPTIMAL SWITCHING FREQUENCY [kHz]  
AND CORRESPONDING COMBINED SYSTEM LOSSES [W].

	2-Level				3-Level			
	SPWM		THPWM		SPWM		THPWM	
	$f_{sw}$	Losses	$f_{sw}$	Losses	$f_{sw}$	Losses	$f_{sw}$	Losses
A	5	4 275	5	4 277	5	4 526	5	4 538
B	11	12 064	9	11 828	8	10 996	10	11 176
C	13	6 293	11	6 218	10	5 465	12	5 617
D	19	4 410	15	4 391	11	3 763	12	3 885
E	10	21 005	6	20 733	6	20 112	9	20 280
F	15	11 992	11	11 899	8	11 188	10	11 356

Fig. 9 provides an example of the inverter, PMSM and combined system losses varying with the switching frequency. The trade-off between inverter losses and PMSM losses becomes visible. For all operating points the loss-optimal switching frequency is lower for the 3-level inverter system compared to the 2-level inverter system.

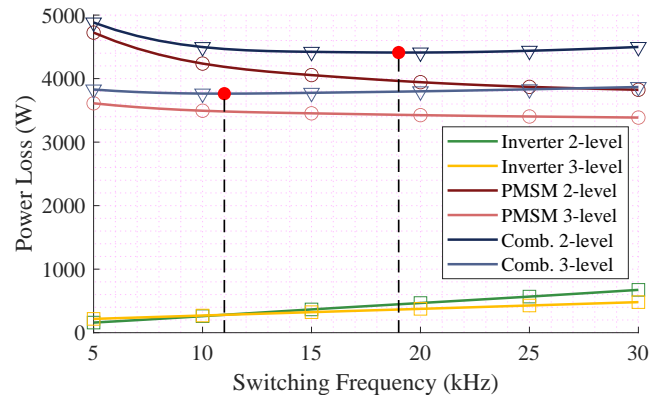


Fig. 9. Inverter, PMSM and Combined Losses using SPWM in operating point D.

TABLE VI

LOSS REDUCTION AT OPTIMAL SWITCHING FREQUENCY COMPARED WITH 2-LEVEL SYSTEM LOSSES OPERATING AT 10 KHZ.

$\Delta_{Loss}$ in:	2-Level				3-Level			
	SPWM		THPWM		SPWM		THPWM	
	[W]	[%]	[W]	[%]	[W]	[%]	[W]	[%]
A	-242	-5	-240	-5	9	0	20	0
B	-9	0	-9	0	-1077	-9	-661	-6
C	-36	-1	-5	0	-864	-14	-605	-10
D	-86	-2	-44	-1	-733	-16	-550	-12
E	0	0	-66	0	-894	-4	-519	-2
F	-72	-1	-2	0	-877	-7	-546	-5

To assess the loss-saving potential, the setup with the 2-level inverter switching at 10kHz is chosen as the reference for comparison. Table VI shows the potential loss savings for all analyzed combinations relative to this reference. While optimizing the switching frequency alone reveals only minor loss saving potential, using a 3-level inverter paired with the PMSM can reduce the system losses by up to 16%.

## V. CONCLUSION

This work evaluates the efficiency trade-off in electric drivetrains between inverter and PMSM losses resulting from PWM operation at various switching frequencies. At preselected operating points, the overall drivetrain efficiency is analyzed, comparing a 2-level and a 3-level inverter setup. Different modulation techniques are tested. The switching frequency is varied in a range of 5 kHz to 30 kHz. It is concluded that depending on the operating point, and the choice of inverter topology and switching strategy, a minimum loss switching frequency in the range of 5 kHz to 19 kHz can be found to maximize overall system energy efficiency. The results reveal that using a 3-level inverter with the optimal switching frequency has significant loss saving potential of up to 1 kW or 16% compared to the 2-level reference system.

## REFERENCES

- [1] Z. Ma, Y. Pei, L. Wang, Q. Yang, Z. Qi, and G. Zeng, "An accurate analytical model of sic mosfets for switching speed and switching loss calculation in high-voltage pulsed power supplies," *IEEE Transactions on Power Electronics*, vol. 38, no. 3, pp. 3281–3297, 2023.
- [2] X. Wang, Z. Zhao, K. Li, Y. Zhu, and K. Chen, "Analytical methodology for loss calculation of sic mosfets," *IEEE Journal of Emerging and Selected Topics in Power Electronics*, vol. 7, no. 1, pp. 71–83, 2019.
- [3] J. Ebersberger, M. Hagedorn, M. Lorenz, and A. Mertens, "Potentials and comparison of inverter topologies for future all-electric aircraft propulsion," *IEEE Journal of Emerging and Selected Topics in Power Electronics*, vol. 10, no. 5, pp. 5264–5279, 2022.
- [4] G. Mörée and M. Leijon, "Iron loss models: A review of simplified models of magnetization losses in electrical machines," *Journal of Magnetism and Magnetic Materials*, vol. 609, p. 172163, 2024.
- [5] D. A. Gonzalez and D. M. Saban, "Study of the copper losses in a high-speed permanent-magnet machine with form-wound windings," *IEEE Transactions on Industrial Electronics*, vol. 61, no. 6, pp. 3038–3045, 2014.
- [6] S. Sirimanna, T. Balachandran, and K. Haran, "A review on magnet loss analysis, validation, design considerations, and reduction strategies in permanent magnet synchronous motors," *Energies*, vol. 15, no. 17, 2022.
- [7] F. Stella, F. Mandrile, S. Musumeci, V. Barba, M. Palma, and A. Acquaviva, "Pwm-induced losses estimation in electrical motor driven with gan-based inverter," in *2024 International Conference on Electrical Machines (ICEM)*. IEEE, 9 2024, pp. 1–6. [Online]. Available: <https://ieeexplore.ieee.org/document/10700058/>
- [8] S. Rubino, F. Mandrile, E. Armando, A. Boglietti, R. Bojoi, A. Carlsson, and S. Nategh, "Impedance-based estimation method of pwm-induced losses for traction motors," in *2023 IEEE International Electric Machines and Drives Conference, IEMDC 2023*. Institute of Electrical and Electronics Engineers Inc., 2023.
- [9] S. Ferrari, P. Ragazzo, G. Dilevrano, and G. Pellegrino, "Flux and loss map based evaluation of the efficiency map of synchronous machines," *IEEE Transactions on Industry Applications*, vol. 59, pp. 1500–1509, 3 2023.
- [10] L. Chang, T. M. Jahns, and R. Blissenbach, "Estimation of pwm-induced iron loss in ipm machines incorporating the impact of flux ripple waveshape and nonlinear magnetic characteristics," *IEEE Transactions on Industry Applications*, vol. 56, pp. 1332–1345, 2020.
- [11] L. Masisi, M. Ibrahim, J. Wanjiku, A. M. Aljehaimi, and P. Pillay, "The effect of two- and three-level inverters on the core loss of a synchronous reluctance machine (synrm)," *IEEE Transactions on Industry Applications*, vol. 52, pp. 3805–3813, 2016.
- [12] M. van der Geest, H. Polinder, and J. A. Ferreira, "Influence of pwm switching frequency on the losses in pm machines," in *2014 International Conference on Electrical Machines (ICEM)*, 2014, pp. 1243–1247.
- [13] N. G. Marmolejo, X. Tang, and M. Doppelbauer, "Influence of different pulse-width modulation methods on magnet losses in permanent magnet synchronous machines," in *2020 22nd European Conference on Power Electronics and Applications (EPE'20 ECCE Europe)*, 2020, pp. P.1–P.10.
- [14] M. Schweizer, T. Friedli, and J. W. Kolar, "Comparative evaluation of advanced three-phase three-level inverter/converter topologies against two-level systems," *IEEE Transactions on Industrial Electronics*, vol. 60, no. 12, pp. 5515–5527, 2013.
- [15] K. Bradley, W. Cao, J. Clare, and P. Wheeler, "Predicting inverter-induced harmonic loss by improved harmonic injection," *IEEE Transactions on Power Electronics*, vol. 23, no. 5, pp. 2619–2624, 2008.
- [16] T. Velic, M. Barkow, D. Bauer, P. Fuchs, J. Wende, T. Hubert, M. Reinlein, J. Nägelkrämer, and N. Parspour, "Efficiency optimization of electric drives with full variable switching frequency and optimal modulation methods," in *2021 17th Conference on Electrical Machines, Drives and Power Systems (ELMA)*, 2021, pp. 1–6.
- [17] J. Azurza Anderson, G. Zulauf, J. W. Kolar, and G. Deboy, "New figure-of-merit combining semiconductor and multi-level converter properties," *IEEE Open Journal of Power Electronics*, vol. 1, pp. 322–338, 2020.
- [18] S. Ferrari, G. Dilevrano, P. Ragazzo, and G. Pellegrino, "The dq-theta flux map model of synchronous machines," in *2021 IEEE Energy Conversion Congress and Exposition, ECCE 2021 - Proceedings*. Institute of Electrical and Electronics Engineers Inc., 2021, pp. 3716–3723.
- [19] R. Jing, G. Wang, G. Zhang, and D. Xu, "Review of field weakening control strategies of permanent magnet synchronous motors," *CES Transactions on Electrical Machines and Systems*, vol. 8, pp. 319–331, 9 2024.
- [20] A. M. Hava, R. J. Kerkman, and T. A. Lipo, "Simple analytical and graphical methods for carrier-based pwm-vsi drives," *IEEE Transactions on Power Electronics*, vol. 14, p. 49, 1999.
- [21] E. Ayaz, M. Jackson, S. Sarmast, B. Singh, S. Norrga, and H.-P. Nee, "Evaluation of possible traction inverter topologies for heavy-duty electric vehicles," in *2024 IEEE 9th Southern Power Electronics Conference (SPEC)*, 2024, pp. 1–6.
- [22] J. Ebersberger, M. Hagedorn, M. Lorenz, and A. Mertens, "Potentials and comparison of inverter topologies for future all-electric aircraft propulsion," *IEEE Journal of Emerging and Selected Topics in Power Electronics*, vol. 10, no. 5, pp. 5264–5279, 2022.
- [23] Z. Wang, Y. Wu, M. H. Mahmud, Z. Zhao, Y. Zhao, and H. A. Mantooth, "Design and validation of a 250-kw all-silicon carbide high-density three-level t-type inverter," *IEEE Journal of Emerging and Selected Topics in Power Electronics*, vol. 8, no. 1, pp. 578–588, 2020.
- [24] H. Zhang, Y. Wu, H. Li, S. Yin, S. Jin, S. Lin, T. Jiang, and Y. Cheng, "Design and evaluation of a 1200-v/200-a sic three-level npc power module," *IEEE Transactions on Industry Applications*, vol. 59, no. 5, pp. 6412–6426, 2023.